JCTC Journal of Chemical Theory and Computation

Article

pubs.acs.org/JCTC

Tensor-Train Split-Operator Fourier Transform (TT-SOFT) Method: Multidimensional Nonadiabatic Quantum Dynamics

Samuel M. Greene and Victor S. Batista*

Department of Chemistry, Yale University, P.O. Box 208107, New Haven, Connecticut 06520-8107, United States

Energy Sciences Institute, Yale University, P.O. Box 27394, West Haven, Connecticut 06516-7394, United States

ABSTRACT: We introduce the "tensor-train split-operator Fourier transform" (TT-SOFT) method for simulations of multidimensional nonadiabatic quantum dynamics. TT-SOFT is essentially the grid-based SOFT method implemented in dynamically adaptive tensor-train representations. In the same spirit of all matrix product states, the tensor-train format enables the representation, propagation, and computation of observables of multidimensional wave functions in terms of the grid-based wavepacket tensor components, bypassing the need of actually computing the wave function in its full-rank tensor product grid space. We demonstrate the accuracy and efficiency of the TT-SOFT method as applied to propagation of 24-dimensional wave packets, describing the S_1/S_2 interconversion dynamics of pyrazine after UV photoexcitation to the S_2 state. Our results show that the TT-SOFT method is a powerful computational approach for simulations of quantum dynamics of polyatomic systems since it avoids the exponential scaling problem of full-rank grid-based representations.

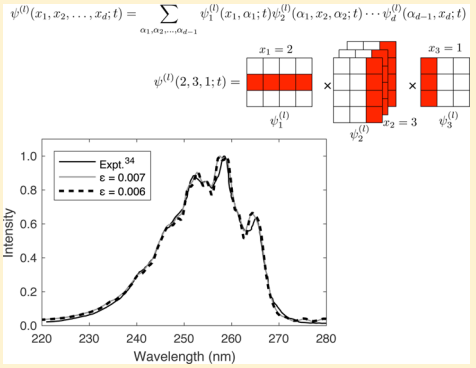

1. INTRODUCTION

A wide range of dynamical processes in chemistry and biology are critically dependent on nonadiabatic quantum effects, including light absorption and photoconversion, electron transfer, and photocatalytic reactions.[1−7] Consequently, there is great interest in the development of first-principles methods to describe nonadiabatic quantum dynamics in systems with many degrees of freedom (DOFs). Here, we introduce the tensor-train split-operator Fourier transform (TT-SOFT) method for efficient, rigorous simulations of nonadiabatic quantum dynamics in polyatomic systems.

The split-operator Fourier transform (SOFT) method is one of the earliest methods developed for numerically exact wave packet propagation.[8−10] While rigorous, the SOFT approach is limited to systems with very few DOFs (i.e., molecular systems with less than 4 or 6 atoms),[11,12] since it requires storage space and computational effort that scale exponentially with the number of coupled DOFs. The exponential scaling challenge has motivated the development of a variety of alternative propagation methods. For example, short iterative Lanczos (SIL) propagation[13] involves projecting the basis into a subspace which facilitates diagonalization algorithms. The Chebyshev polynomial expansion method involves performing a series expansion of the time-evolution operator in a basis of Chebyshev polynomials.[12,14,15] These approaches enable some improvements in efficiency, but the size of the underlying basis nevertheless scales exponentially with the dimensionality of the system. Other methods implement semiclassical approximations.[16−19]

A variety of methods have been developed to address the exponential scaling issue by truncating the basis set. Many of these methods use Gaussian basis states, including the method of coupled coherent states,[20,21] the matching-pursuit algorithm,[22] and multiple-spawning.[23,24] The Multi-configurational time-dependent Hartree (MCTDH) method groups DOFs into "particles" and represents them in a DVR basis.[11,25−29] The use of a small number of basis functions per particle and multilayer implementations have made the MCTDH method computationally efficient.[30,31] MCTDH has been used to treat various systems with many DOFs, including the 24-dimensional wave packet describing the S_1/S_2 interconversion dynamics of pyrazine after UV photoexcitation.[32]

For most of these methods, however, determining exactly how to truncate the basis for general purpose applications is difficult and requires system-specific analyses, iterative methods, or ad hoc approximations. For example, multiple-spawning methods use classical trajectories to determine the location of newly spawned basis functions.[24] In MCTDH, the choice of how DOFs should be grouped into particles involves ad hoc user input and should be based on which DOFs are most strongly coupled. Therefore, the truncation scheme can be difficult to determine a priori.[29] Furthermore, the differential equations of motion used to evolve the single-particle basis functions in MCTDH are strongly coupled, and their solution therefore requires special integration techniques.[29]

Received: June 11, 2017
Published: August 1, 2017

DOI: 10.1021/acs.jctc.7b00608
J. Chem. Theory Comput. XXXX, XXX, XXX−XXX

A more systematic approach for propagating multidimensional wave packets in a truncated basis has been introduced with the development of the "matching pursuit split-operator Fourier transform" (MP-SOFT) method.[33−35] The MP-SOFT methodology is based on the recursive application of the time evolution operator, as given by the Trotter expansion to second order accuracy, using a dynamically adaptive coherent-state representation generated by the matching-pursuit algorithm.[36] An advantage of this approach is the systematic approach to dynamically adapting the representation, namely, by minimizing the residual amplitude after each propagation step subject to the constraint of a desired accuracy. The main disadvantage of MP-SOFT is the computational expense involved in regenerating the matching pursuit coherent-state expansion after each propagation step.

The TT-SOFT method is inspired by MP-SOFT. However, rather than representing the time-evolving wave packet in terms of a matching pursuit coherent state expansion, TT-SOFT represents the wave packet in an adaptive tensor-train format generated by sequential singular value decompositions.[37] Like MP-SOFT, the TT-SOFT approach does not rely on ad hoc or user decisions other than a single accuracy parameter. An advantage of TT-SOFT when compared to MP-SOFT is that it minimizes the residual amplitude after each propagation step very efficiently through a series of QR decompositions[38] followed by rank truncation based on sequential singular value decomposition. This approach provides a systematic procedure to adapt the representation as the wave function evolves in time. It is worth noting that the tensor-train format is a special case of the hierarchical Tucker format employed in the multilayer implementation of MCTDH.[30] However, the key distinction between TT-SOFT and MCTDH, apart from the integration scheme, is the adaptability of the size of the basis in TT-SOFT.

In the same spirit of all matrix product states, the tensor-train format enables the representation, propagation, and computation of observables of multidimensional wave functions by operating only with the core tensor *components*, bypassing the need of computing the wave function in its exponentially large full-rank tensor product grid space. TT-SOFT thus enables the implementation of the SOFT propagation scheme in full-dimensionality, subject to the constraint of a specified accuracy, while retaining the advantages of a grid-based representation method (e.g., the ease of representing any arbitrary potential or wave function and the lack of ad hoc approximations in the construction of the basis).

We illustrate the TT-SOFT method as applied to simulations of nonadiabatic quantum dynamics for a system with many nuclear DOFs evolving on two electronically coupled states. We focus on the S_1/S_2 interconversion of pyrazine, which is an ideal model system since it allows for direct comparisons with previous theoretical studies[20,29,39−44] and experimental work.[45−49] Pyrazine is characterized by a conical intersection between the S_1 and the S_2 states and strong vibronic couplings that enable ultrafast intersystem crossing, giving rise to a broad photoabsorption spectrum with vibronic features. Due to the nonadiabaticity of the dynamics, pyrazine can prove difficult to study with quantum dynamics simulations and, therefore, serves as a rigorous test of the accuracy and capabilities of propagation methods.[29]

2. METHODS

2.1. TT-SOFT Method. In TT-SOFT, the time-evolved wave function,

$$\Psi(\mathbf{x}, t_0 + \tau) = \int d\mathbf{x}' \langle \mathbf{x}| e^{-i\hat{H}\tau/\hbar} |\mathbf{x}'\rangle \Psi(\mathbf{x}', t_0) \tag{1}$$

is calculated by representing $\Psi(\mathbf{x}', t_0)$ as described in Section 2.3.1, as a tensor train,[37] and applying the short-time approximation of the time-evolution operator given by the Trotter expansion:

$$e^{-i\hat{H}\tau/\hbar} = e^{-i\hat{T}\tau/2\hbar} e^{-i\hat{V}\tau/\hbar} e^{-i\hat{T}\tau/2\hbar} + O(\tau^3) \tag{2}$$

Here, the Hamiltonian is

$$\hat{H} = \hat{T} + \hat{V} \tag{3}$$

where $\hat{T} = \frac{1}{2}\hat{\mathbf{p}}\cdot\mathbf{m}^{-1}\cdot\hat{\mathbf{p}}$ is the kinetic energy operator, $\hat{\mathbf{p}}$ is the momentum operator, $\mathbf{m}$ is the diagonal matrix of masses, and $\hat{V}$ is the potential energy operator, which is assumed to be time-independent during the propagation time step τ.

Substituting the Trotter expansion, introduced by eq 2, into eq 1 and inserting the closure relations, $1 = \int d\mathbf{p}|\mathbf{p}\rangle\langle\mathbf{p}|$, $1 = \int d\mathbf{x}''|\mathbf{x}''\rangle\langle\mathbf{x}''|$, and $1 = \int d\mathbf{p}'|\mathbf{p}'\rangle\langle\mathbf{p}'|$, yields

$$\begin{aligned}\Psi(\mathbf{x}, t_0 + \tau) &= \int d\mathbf{x}' \langle \mathbf{x}| e^{-i\hat{\mathbf{p}}\cdot\mathbf{m}^{-1}\cdot\hat{\mathbf{p}}\tau/4\hbar} e^{-i\hat{V}\tau/\hbar} e^{-i\hat{\mathbf{p}}\cdot\mathbf{m}^{-1}\cdot\hat{\mathbf{p}}\tau/4\hbar} |\mathbf{x}'\rangle \Psi(\mathbf{x}', t_0) \\ &= \int d\mathbf{p} \langle \mathbf{x}|\mathbf{p}\rangle e^{-i\mathbf{p}\cdot\mathbf{m}^{-1}\cdot\mathbf{p}\tau/4\hbar} \int d\mathbf{x}'' \langle \mathbf{p}|\mathbf{x}''\rangle e^{-iV(\mathbf{x}'')\tau/\hbar} \\ &\quad \times \int d\mathbf{p}' \langle \mathbf{x}''|\mathbf{p}'\rangle e^{-i\mathbf{p}'\cdot\mathbf{m}^{-1}\cdot\mathbf{p}'\tau/4\hbar} \int d\mathbf{x}' \langle \mathbf{p}'|\mathbf{x}'\rangle \Psi(\mathbf{x}', t_0)\end{aligned} \tag{4}$$

where $\langle \mathbf{x}|\mathbf{p}\rangle = (2\pi\hbar)^{-d/2} e^{i\mathbf{p}\cdot\mathbf{x}/\hbar}$, with d the number of DOFs. Because the integrals in eq 4 are Fourier transform (FT) or inverse Fourier transform (IFT), the propagation can be summarized, as follows:

$$\begin{aligned}&\Psi(\mathbf{x}, t_0 + \tau) \\ &= \mathrm{IFT}[e^{-i\mathbf{p}\cdot\mathbf{m}^{-1}\cdot\mathbf{p}\tau/4\hbar} \mathrm{FT}[e^{-i\hat{V}(\mathbf{x}'')\tau/\hbar} \mathrm{IFT}[e^{-i\mathbf{p}\cdot\mathbf{m}^{-1}\cdot\mathbf{p}\tau/4\hbar} \\ &\quad \times \mathrm{FT}[\Psi(\mathbf{x}', t_0)]]]]\end{aligned} \tag{5}$$

Propagation over a time interval τ is thus accomplished by first Fourier transforming the initial wave function, represented in position space, using the fast Fourier transform (FFT) algorithm.[38] The resulting momentum-space wave function is then multiplied by the free-particle propagator. The result is then inverse Fourier-transformed and multiplied by $e^{-iV(\mathbf{x}'')\tau/\hbar}$. Finally, this position−space wave function is Fourier transformed and multiplied by the free-particle propagator. The inverse Fourier transform completes a propagation step. The wave function at time $t = t_0 + N\tau$ is obtained by repeating this procedure N times.

2.2. Two-Level Multidimensional Vibronic Model. The TT-SOFT method can be implemented to simulate nonadiabatic quantum dynamics for a d-dimensional vibronic system evolving on an arbitrarily large number of coupled electronic states. For simplicity, here, we illustrate its implementation as applied to the description of pyrazine evolving on 2-coupled electronic states, described by the Hamiltonian introduced by eq 3 with the kinetic energy operator,

DOI: 10.1021/acs.jctc.7b00608
J. Chem. Theory Comput. XXXX, XXX, XXX−XXX

$$\hat{T} = \sum_{j=1}^{d} \frac{\hat{p}_j^2}{2m_j}(|1\rangle\langle 1| + |2\rangle\langle 2|) \tag{6}$$

where d is the number of nuclear coordinates x_j (i.e., normal modes) with effective masses m_j and momenta $\hat{p}_j$. The states $|1\rangle$ and $|2\rangle$ are the two coupled electronic states. $\hat{V}$, introduced by eq 3, is the sum of diabatic and coupling potential energy operators,

$$\hat{V} = \hat{V}_d + \hat{V}_c \tag{7}$$

where $\hat{V}_d = \hat{V}_1 + \hat{V}_2$ is the sum of the vibronic multimode expansions describing the potential energy surfaces for each electronic state, parametrized as follows for pyrazine:[29]

$$\hat{V}_k = \left(E_k + \sum_{j=1}^{d} \frac{1}{2} m_j \omega_j x_j^2 + \sum_{i=1}^{d} a_i^k x_i + \sum_{i=1}^{d}\sum_{j=1}^{d} a_{ij}^k x_i x_j\right)|k\rangle\langle k| \tag{8}$$

E_k represents the energy of the system in state $|k\rangle$ for all $x_j = 0$. The frequencies ω_j and normal mode eigenvectors are those for the system in a reference electronic state (in this case, the ground state). The remaining parameters (a_i^k and a_{ij}^k) correspond to linear and bilinear couplings. Finally, the $\hat{V}_c$ operator accounts for vibronic couplings between electronic states, as follows:

$$\hat{V}_c = \left(\sum_{i=1}^{d} c_i x_i + \sum_{i=1}^{d}\sum_{j=1}^{d} c_{ij} x_i x_j\right)(|1\rangle\langle 2| + |2\rangle\langle 2|) \tag{9}$$

With these definitions, the total Hamiltonian matrix is

$$H = T + V \tag{10}$$

where $T_{kk'} = \delta_{kk'} \sum_{j=1}^{d} \frac{\hat{p}_j^2}{2m_j}$, $V_{kk} = E_k + \sum_{j=1}^{d} \frac{1}{2} m_j \omega_j x_j^2 + \sum_{i=1}^{d} a_i^k x_i + \sum_{i=1}^{d}\sum_{j=1}^{d} a_{ij}^k x_i x_j$, and $V_{kk'} = \sum_{i=1}^{d} c_i x_i + \sum_{i=1}^{d}\sum_{j=1}^{d} c_{ij} x_i x_j$, when $k \neq k'$. Each of these matrix elements are d-dimensional tensor-trains, constructed as described in Section 2.4.

The propagator is obtained as a function of the nuclear coordinates $\mathbf{x}$ through its truncated power series expansion:

$$e^{-iV\tau/\hbar} = \sum_{n=0}^{N} \frac{(-iV\tau/\hbar)^n}{n!} \tag{11}$$

where N is chosen to be sufficiently large ($N = 10$ in this study) to ensure convergence of the power series. The series on the r.h.s. of eq 11 involves powers of matrices of d-dimensional tensor-trains. Further discussion of the numerical procedures used to calculate this power series can be found in Section 2.3.3.

According to eq 5, the time-evolving wave function $\Psi(\mathbf{x}, t)$ is represented in coordinate space as a column vector of tensor trains corresponding to nuclear wave functions for each electronic state, as follows:

$$\Psi(\mathbf{x}, t) = \begin{pmatrix} \psi^{(1)}(\mathbf{x}, t) \\ \psi^{(2)}(\mathbf{x}, t) \end{pmatrix} \tag{12}$$

$\psi^{(1)}(\mathbf{x}, t)$ and $\psi^{(2)}(\mathbf{x}, t)$ are Fourier transformed to generate tensor trains in momentum space $\tilde{\psi}^{(i)}(\mathbf{p}, t)$. These are each multiplied by the free particle propagator $e^{-i\mathbf{p}\cdot\mathbf{m}^{-1}\cdot\mathbf{p}\tau/4\hbar}$, in the form of a rank-1 tensor train in momentum space, to obtain $\tilde{\psi}'^{(i)}(\mathbf{p}, t)$. The inverse Fourier transform of $\tilde{\psi}'^{(i)}(\mathbf{p}, t)$ yields the wave functions $\psi'^{(i)}(\mathbf{x}, t)$ which are then operated upon by $e^{-iV\tau/\hbar}$:

$$\begin{pmatrix} \psi''^{(1)}(\mathbf{x}, t) \\ \psi''^{(2)}(\mathbf{x}, t) \end{pmatrix} = e^{-iV\tau/\hbar} \begin{pmatrix} \psi'^{(1)}(\mathbf{x}, t) \\ \psi'^{(2)}(\mathbf{x}, t) \end{pmatrix} \tag{13}$$

which involves matrix multiplication (i.e., multiplication and addition of tensor trains) as in eq 11. The Fourier transforms of $\psi''^{(1)}(\mathbf{x}, t)$ and $\psi''^{(2)}(\mathbf{x}, t)$ yield $\tilde{\psi}''^{(1)}(\mathbf{p}, t)$ and $\tilde{\psi}''^{(2)}(\mathbf{p}, t)$ which can be used to complete the propagation step by first multiplying them by $e^{-i\mathbf{p}\cdot\mathbf{m}^{-1}\cdot\mathbf{p}\tau/4\hbar}$ to obtain $\tilde{\psi}^{(i)}(\mathbf{p}, t + \tau)$ and then performing an inverse Fourier transform.

2.3. Tensor-Train Implementation.

2.3.1. TT Format. The tensor-train (TT) representation of any d-dimensional tensor A is defined, as follows:[37]

$$A(i_1, i_2, ..., i_d) = \sum_{\alpha_1=1}^{r_1} \sum_{\alpha_2=1}^{r_2} \cdots \sum_{\alpha_{d-1}=1}^{r_{d-1}} A_1(i_1, \alpha_1) A_2(\alpha_1, i_2, \alpha_2) \cdots A_d(\alpha_{d-1}, i_d) \tag{14}$$

where the indices $\mathbf{i} = (i_1, i_2, ..., i_d)$ label the physical dimensions. The tensors A_k are called *cores*, each of which is associated with only one physical dimension. The *auxiliary indices* α_k connect the cores by matrix multiplication, forming a *train* (i.e., a linear chain of tensors). The maximum value of the kth physical index will be denoted n_k, and the maximum value of the kth auxiliary index (i.e., the kth rank) is denoted r_k. Equation 14 can be expressed alternatively as a product of matrices:

$$A(i_1, i_2, ..., i_d) = A_1(i_1) A_2(i_2) \cdots A_d(i_d) \tag{15}$$

where $A_k(i_k)$ is an $r_{k-1} \times r_k$ matrix. The conditions $r_0 = r_d = 1$ are imposed, as $A(i_1, i_2, ..., i_d)$ represents a scalar. Equation 15 clearly shows that the tensor-train format is a generalized form of factorization of the d-dimensional tensor as a *matrix-product state*, where each matrix depends on a single dimension.

An example is the TT representation of the d-dimensional wave packet $\psi^{(l)}(\mathbf{x}, t)$ with physical coordinate indices, $\mathbf{x} = (x_1, x_2, ..., x_d)$:

$$\psi^{(l)}(x_1, x_2, ..., x_d; t) = \sum_{\alpha_1, \alpha_2, ..., \alpha_{d-1}} \psi_1^{(l)}(x_1, \alpha_1; t) \psi_2^{(l)}(\alpha_1, x_2, \alpha_2; t) \cdots \psi_d^{(l)}(\alpha_{d-1}, x_d; t) \tag{16}$$

Another example is the TT representation of the free particle propagator $U(\mathbf{p}) = e^{-i\mathbf{p}\cdot\mathbf{m}^{-1}\cdot\mathbf{p}\tau/2\hbar}$, with physical indices in momentum space, $\mathbf{p} = (p_1, p_2, ..., p_d)$:

$$U(p_1, p_2, ..., p_d) = \sum_{\alpha_1, \alpha_2, ..., \alpha_{d-1}} U_1(p_1, \alpha_1) U_2(\alpha_1, p_2, \alpha_2) \cdots U_d(\alpha_{d-1}, p_d) \tag{17}$$

2.3.2. Tensor Kronecker Products: Initial State and Free Particle Propagator. The nuclear wave packet of pyrazine is initialized in the optically active S_2 state as a product of 1-dimensional wave functions, each of which is the harmonic oscillator ground state wave function for a normal mode of the molecule in its ground electronic state:

DOI: 10.1021/acs.jctc.7b00608
J. Chem. Theory Comput. XXXX, XXX, XXX−XXX

$$\psi^{(1)}(\mathbf{x};\, t_0) = 0$$
$$\psi^{(2)}(\mathbf{x};\, t_0) = \prod_{j=1}^{d} \psi_j^{(2)}(x_j;\, t_0) \tag{18}$$

where $\psi_j^{(2)}(x_j;\, t_0) = \left(\frac{1}{\pi}\right)^{1/4} e^{-1/2x_j^2}$ and d is the number of nuclear DOFs (i.e., $d = 4$ for the reduced-mode benchmark calculation and $d = 24$ for the full-dimensional calculation). Since the d-dimensional wave function $\psi^{(2)}(\mathbf{x};t_0)$ is a product of 1-dimensional wave functions, its TT representation is the *tensor Kronecker product*,[50]

$$\psi^{(2)}(x_1, x_2, ..., x_d;\, t_0) = \sum_{\alpha_1=1}^{1} \sum_{\alpha_2=1}^{1} \cdots \sum_{\alpha_{d-1}=1}^{1} \psi_1^{(2)}(x_1, \alpha_1;\, t_0)\psi_2^{(2)}(\alpha_1, x_2, \alpha_2;\, t_0) \cdots \psi_d^{(2)}(\alpha_{d-1}, x_d;\, t_0) \tag{19}$$

which is a rank-1 tensor train. Each core $\psi_j^{(2)}$ in eq 19 consists of an array (i.e., column vector) corresponding to the jth 1-dimensional component of the wave function introduced by eq 18. The TT representation of $\psi^{(1)}(\mathbf{x};\, t_0)$ is also rank-1, with column vectors of zeros.

The free particle propagator is also a product of 1-dimensional functions, in momentum space:

$$e^{-i\mathbf{p}\cdot\mathbf{m}^{-1}\cdot\mathbf{p}\tau/2\hbar} = \prod_{j=1}^{d} e^{-ip_i^2\tau/2m_i\hbar} \tag{20}$$

and therefore is constructed analogously, in TT format, as a tensor Kronecker product.

2.3.3. Propagation: Elementwise Multiplication and Addition. The TT-SOFT propagation method, introduced in Section 2.1, requires multiplication of tensor trains associated with the time-evolving wave packet, the free particle propagator $e^{-i\mathbf{p}\cdot\mathbf{m}^{-1}\cdot\mathbf{p}\tau/2\hbar}$, and the matrix elements of $e^{-iV(\mathbf{x})\tau/\hbar}$ introduced by eq 11. The multiplication of tensor trains A and B involves taking the elementwise product (i.e., Hadamard product)[50] of the two tensors, as follows:

$$D(i_1, i_2, ..., i_d) = A(i_1, i_2, ..., i_d)B(i_1, i_2, ..., i_d) \tag{21}$$

where A and B must have the same dimensions. In matrix format, the TT cores of their Hadamard product are given as follows:[37]

$$D_k(i_k) = A_k(i_k) \otimes B_k(i_k) \tag{22}$$

where $\otimes$ denotes the matrix Kronecker product of $A_k(i_k)$ and $B_k(i_k)$.[50] If the dimensions of the cores A_k and B_k are $r_{k-1}^{(a)} \times n_k \times r_k^{(a)}$ and $r_{k-1}^{(b)} \times n_k \times r_k^{(b)}$, respectively, then the dimensions of the resulting core D_k are $(r_{k-1}^{(a)}\, r_{k-1}^{(b)}) \times n_k \times (r_k^{(a)}\, r_k^{(b)})$.

Tensor trains must be added in order to perform the matrix multiplication in eqs 11 and 13. The sum of two tensors A and B with the same dimensions is defined analogously to the elementwise product, as follows:

$$E(i_1, i_2, ..., i_d) = A(i_1, i_2, ..., i_d) + B(i_1, i_2, ..., i_d) \tag{23}$$

The TT cores of E are given in matrix format in terms of the cores of A and B, as follows:[37]

$$E_k(i_k) = \begin{pmatrix} A_k(i_k) & 0 \\ 0 & B_k(i_k) \end{pmatrix} \tag{24}$$

for $1 < k < d$ and

$$E_1(i_1) = \begin{pmatrix} A_1(i_1) & B_1(i_1) \end{pmatrix} \tag{25}$$

and

$$E_d(i_d) = \begin{pmatrix} A_d(i_d) \\ B_d(i_d) \end{pmatrix} \tag{26}$$

Thus, the ranks of E are equal to the sums of the ranks of A and B.

The propagator is calculated by elementwise multiplication and addition, implementing the scaling and squaring method,[51] as follows: $e^{-iV\tau/\hbar} = (e^{-iV\tau/2^s\hbar})^{2^s}$ with s an integer scaling parameter that ensures rapid convergence of the Taylor series of $e^{-iV\tau/2^s\hbar}$. Upon convergence, the series is squared s times to obtain the propagator. The construction of the d-dimensional tensor trains corresponding to the matrix elements of V (introduced by eq 10) is discussed in Section 2.4. Each of these tensor trains is then multiplied by a constant, $c = (-i\tau/\hbar)$, which simply involves multiplying the elements of one of the cores by c. Subsequently, the matrix $(-iV\tau/\hbar)$ is divided by 2^s, with the scaling parameter s chosen to ensure that none of the elements of the tensor-train components of the matrix $(-iV\tau/2^s\hbar)$ has a magnitude greater than 0.5. The exponential of this scaled matrix is then computed using a Taylor series, with as many terms as is needed to ensure convergence of the series to within an accuracy indicated by the parameter ε (eq 31).

2.3.4. Truncation: Rounding. The multiplications and additions required by TT-SOFT propagation increase the ranks of the TT representation, as described in Section 2.3.3. Therefore, we implement a rounding algorithm to reduce the ranks after each propagation step.[37] First, a QR decomposition is applied to the first core A_1 of the TT representation, giving

$$A_1(i_1, \alpha_1) = \sum_{\alpha_1'=1}^{r_1'} Q_1(i_1, \alpha_1')R_1(\alpha_1', \alpha_1) \tag{27}$$

where the matrix A_1 is expressed as a product of matrices Q_1 and R_1, with Q_1 a matrix of orthonormal column vectors and R_1 an upper triangular matrix. The elements of the matrix R_1 are divided by the norm of R_1 (i.e., the sum of the squares of its elements), denoted f_2, to yield a normalized matrix R_1'.

The second core of the TT tensor to be rounded, A_2, is then unfolded into a matrix A_2' of size $(r_1) \times (n_2 r_2)$, as follows:[50]

$$A_2'(\alpha_1, j) = A(\alpha_1, i_2, \alpha_2) \tag{28}$$

where

$$j = i_2 + (\alpha_2 - 1)r_2 \tag{29}$$

Tensor unfolding and, analogously, matrix refolding can be efficiently performed, for example, using the `reshape` subroutine of MATLAB. A_2' is then left-multiplied by the matrix R_1'. A QR decomposition is performed on the resulting matrix to yield matrices Q_2 and R_2'. This process is repeated iteratively until the last core, A_d, is left-multiplied by the normalized matrix R_{d-1}', to yield matrix Q_d, with dimensions $r_{d-1}' \times n_d$.

DOI: 10.1021/acs.jctc.7b00608
J. Chem. Theory Comput. XXXX, XXX, XXX−XXX

Following this series of QR decompositions, a series of singular value decompositions (SVDs) is applied to the resulting matrices Q_i. SVD is a generalization of matrix diagonalization to nonsquare matrices. The first SVD is performed to express Q_d as a product of matrices U, S, and V, as follows:

$$Q_d(\alpha'_{d-1}, i_d) = \sum_{\alpha''_{d-1}=1}^{r''_{d-1}} U(\alpha'_{d-1}, \alpha''_{d-1}) S(\alpha''_{d-1}, \alpha''_{d-1}) V^{\mathrm{T}} (\alpha''_{d-1}, i_d) \tag{30}$$

or in matrix form, $Q_d = USV^{\mathrm{T}}$, where S is a diagonal matrix of singular values, and the matrices U and V are unitary. The matrix V^{T} defines the last core of the tensor train, associated with the physical dimension d. Then, Q_{d-1} is reshaped into a matrix with dimensions $(r'_{d-2}\ n_{d-1}) \times (r'_{d-1})$ and is right-multiplied by the matrix product US. The resulting matrix is reshaped with dimensions $(r'_{d-2}) \times (n_{d-1}\ r''_{d-1})$, and an SVD is applied. These steps are repeated until the matrix product US obtained from Q_2 is left-multiplied by Q_1. This core is divided by its norm, f_1, and each of the cores are then multiplied by the geometric mean of the norms f_1, f_2, ..., f_d to yield the TT representation.

The SVD is a key aspect of the TT-SOFT method since it allows the tensor train to be truncated by zeroing the singular values $S(\alpha_k, \alpha_k) \leq \delta$, with δ defined in terms of the user-specified accuracy parameter ε, as follows:[37]

$$\delta = \frac{\varepsilon}{\sqrt{d-1}} \tag{31}$$

Thus, the accuracy parameter determines the ranks r_k of the rounded TT representation, the size of which typically scales subexponentially with the number of degrees of freedom.

2.3.5. Fourier Transform of Tensor Trains. The Fourier transform of the d-dimensional tensor train $\psi^{(l)}(\mathbf{x}; t)$ is defined, as follows:

$$\tilde{\psi}^{(l)}(p_1, p_2, ..., p_d; t) = \sum_{\alpha_1,\alpha_2,\cdots\alpha_{d-1}} (2\pi\hbar)^{-d/2} \times \int d\mathbf{x} e^{-i\mathbf{x}\cdot\mathbf{p}/\hbar} \psi_1^{(l)}(x_1, \alpha_1; t) \psi_2^{(l)}(\alpha_1, x_2, \alpha_2; t) \cdots \psi_d^{(l)}(\alpha_{d-1}, x_d; t), \tag{32}$$

where, for notational simplicity, the discrete indices x_i are treated as continuous variables. Since each core $\psi_i^{(l)}$ depends on only one index x_i, the above integral can be factorized as a product of 1-dimensional integrals, as follows:

$$\begin{aligned}\tilde{\psi}^{(l)}(p_1, p_2, ..., p_d; t) = \sum_{\alpha_1,\alpha_2,...,\alpha_{d-1}} & (2\pi\hbar)^{-1/2} \int dx_1 e^{-ix_1p_1/\hbar} \psi_1^{(l)}(x_1, \alpha_1; t) \\ & \times (2\pi\hbar)^{-1/2} \int dx_2 e^{-ix_2p_2/\hbar} \psi_2^{(l)}(\alpha_1, x_2, \alpha_2; t) \times \\ & \cdots \times (2\pi\hbar)^{-1/2} \int dx_d e^{-ix_dp_d/\hbar} \psi_d^{(l)}(\alpha_{d-1}, x_d; t)\end{aligned} \tag{33}$$

These integrals comprise the cores of the Fourier transformed TT representation:

$$\begin{aligned}\tilde{\psi}^{(l)}(p_1, p_2, ..., p_d; t) = & \sum_{\alpha_1,\alpha_2,\ldots\alpha_{d-1}} \tilde{\psi}_1^{(l)}(p_1, \alpha_1; t) \tilde{\psi}_2^{(l)}(\alpha_1, p_2, \alpha_2; t) \\ & \cdots \tilde{\psi}_d^{(l)}(\alpha_{d-1}, p_d; t)\end{aligned} \tag{34}$$

Thus, the Fourier transform of $\tilde{\psi}^{(l)}(\mathbf{x}; t)$ can be obtained by unfolding each of its cores $\psi_k^{(l)}$ into a $(n_k) \times (r_k\ r_{k+1})$ matrix and then Fourier transforming each of the column vectors of the resulting matrices by using the FFT algorithm.

2.3.6. Survival Amplitude: Dot Product Tensor-Train Contraction. The photoabsorption spectrum of pyrazine is calculated as the Fourier transform of the time-dependent survival amplitude:[29]

$$C(t - t_0) = \langle \Psi(t_0) | \Psi(t) \rangle \tag{35}$$

which is calculated as the dot product of the initial wave function corresponding to the S_2 electronic state, $\psi^{(2)}(\mathbf{x}; t_0)$, and the propagated wave function $\psi^{(2)}(\mathbf{x}; t)$, since initially there is no population in the S_1 state.

The dot product of tensor trains A and B is defined, as follows:

$$\sum_{i_1=1}^{n_1} \sum_{i_2=1}^{n_2} \cdots \sum_{i_d=1}^{n_d} A^*(i_1, i_2, ..., i_d) B(i_1, i_2, ..., i_d) \tag{36}$$

When A and B are represented in TT format, the dot product is obtained by first calculating $A_1^\dagger B_1$, which is a matrix with size $r_1^{(a)} \times r_1^{(b)}$. $A_1^\dagger$ denotes the complex transpose of core A_1. The core B_2 is refolded into a matrix of size $(r_1^{(b)}) \times (n_2 r_2^{(b)})$ and left-multiplied by $A_1^\dagger$ B_1 to yield a matrix of size $(r_1^{(a)}) \times (n_2 r_2^{(b)})$. This resulting matrix is refolded and transposed to give a matrix of size $(r_2^{(b)}) \times (r_1^{(a)} n_2)$. This is right-multiplied by the core A_2^* refolded into a matrix of size $(r_1^{(a)} n_2) \times (r_2^{(a)})$. The transpose of this result is a matrix of size $r_2^{(a)} \times r_2^{(b)}$. This algorithm is repeated iteratively until multiplication by the dth cores of A and B yields a scalar, which is the desired dot product.[37]

2.3.7. Parallelization. The multiplication, addition, and Fourier transform operations of tensors in TT format involve manipulating single cores or pairs of cores. Therefore, many TT operations are particularly conducive to trivial parallelization. The cores of the TT representation of a wave function can be stored separately in computer memory, which facilitates the application of distributed computing frameworks to TT operations. In this study, we utilized the MATLAB Parallel Computing Toolbox to perform distributed calculations.

2.4. Potential Energy Surfaces of Pyrazine. The Hamiltonian of pyrazine is defined according to eqs 8 and 9, parametrized as previously reported at the complete active space self-consistent field (CASSCF) level of theory.[32] The potential energy surfaces are shifted by 4.18 and 2.47 eV in the 4- and 24-dimensional calculations, respectively, consistently with the energy of the excited states of pyrazine relative to the ground state. The terms of eqs 8 and 9 that involve only one nuclear coordinate, x_i, are obtained as d-dimensional tensor Kronecker products. The elements of the ith core correspond to the values of x_i multiplied by the appropriate potential parameter, and the elements of the other cores are all ones. TT representations of potential terms that contain products of two nuclear coordinates, x_ix_j, are constructed analogously as tensor Kronecker products, with the ith and jth cores representing values of x_i and x_j, respectively. The elements of the remaining cores are ones, and the entire tensor train is multiplied by the

DOI: 10.1021/acs.jctc.7b00608
J. Chem. Theory Comput. XXXX, XXX, XXX−XXX

potential parameter. The appropriate tensor trains are added to yield d-dimensional TT representations of $\hat{V}_1(\mathbf{x})$, $\hat{V}_2(\mathbf{x})$, and $\hat{V}_c(\mathbf{x})$. Numerical tests suggested that ordering the coordinates such that more strongly coupled DOFs are closer to each other in the TT representation generally improved the algorithm's efficiency.

2.5. Photoabsorption Spectrum. The photoabsorption spectrum, $I(\omega)$, is calculated from the Fourier transform of the complex-valued survival amplitude $C(t)$, introduced by eq 35, as follows:[29,32]

$$I(\omega) \propto \omega \int_{-\infty}^{\infty} dt C(t) e^{i\omega t} \tag{37}$$

To facilitate the comparison with the experimental spectrum, we damp $C(t)$ exponentially with a phenomenological dephasing time τ_h, as follows:[29,32]

$$h(t) = e^{-|t|/\tau_h} \tag{38}$$

which is equivalent to the convolution of the calculated spectrum with a Lorentzian to account for homogeneous broadening. The value of τ_h = 150 fs is used for 24-dimensional calculations, and τ_h = 30 fs is used for 4-dimensional calculations.[32,52] Additionally, $C(t)$ is multiplied by the following function:

$$g(t) = \cos\left(\frac{\pi t}{2T}\right) \tag{39}$$

where T is the total simulation time (165 fs in this study), to avoid artificial ripple effects associated with the Fourier transform introduced by eq 37 (i.e., the Gibbs phenomenon).[32] All spectra are scaled to have a maximum intensity equal to 1.

3. RESULTS

We have assessed the accuracy and efficiency of the TT-SOFT method with respect to the value of the accuracy parameter, ε, as applied to benchmark 4-dimensional wavepacket propagation at the S_1/S_2 conical intersection of pyrazine and direct comparisons to SOFT calculations based on the standard full-rank grid-based implementation (Figure 1). In both TT-SOFT and SOFT calculations, the wave function and propagators are represented with the same grid basis set, with 16 grid-points per dimension.

Figure 1 shows that the TT-SOFT calculations with $\varepsilon < 0.02$ are in excellent agreement with benchmark SOFT calculations and almost completely converged with ε = 0.02. In fact, the spectrum calculated with ε = 0.02 exhibits only slight deviations at wavelengths of 260−265 nm, also reflected in the survival amplitudes.

Figure 2 shows that TT-SOFT simulations are significantly more efficient than SOFT calculations, as shown for example by the memory requirement as a function of time determined by the total numbers of tensor elements in the TT representations (i.e., the "sizes" of the tensor trains) of the nuclear wave functions corresponding to the S_1 and S_2 electronic states for 4-dimensional TT-SOFT simulations. The numbers of elements in all of these wave functions are significantly less (by at least an order of magnitude) than in the full-rank SOFT representation with 16^4 = 65536 elements. We also note that the couplings among nuclear and electronic degrees of freedom generally increase the ranks of the time evolving wavepackets and, therefore, the sizes of the wave functions as they evolve in time,

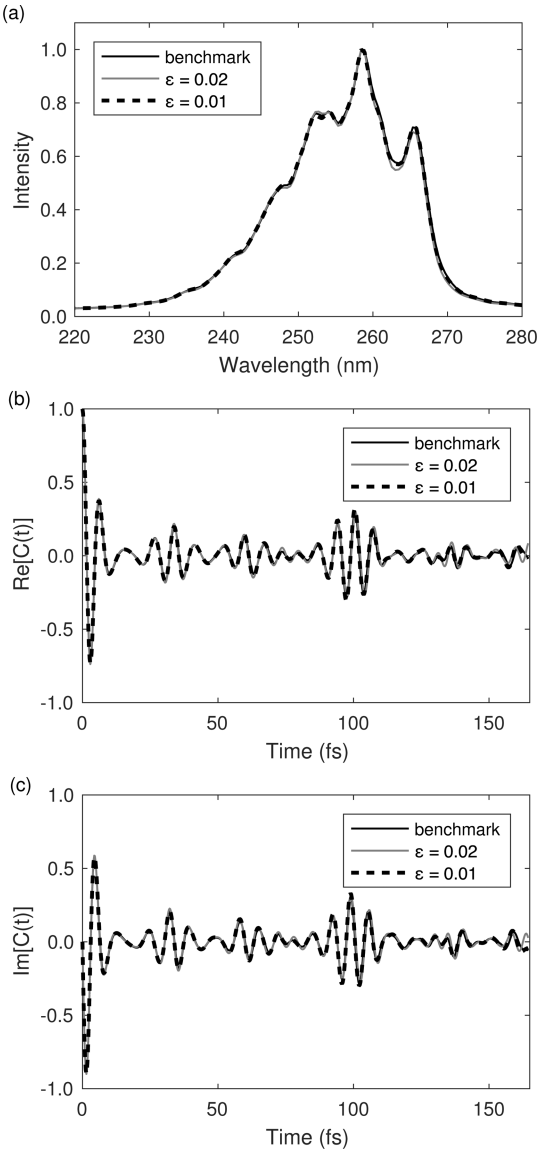

Figure 1. Comparison of TT-SOFT and SOFT (solid black line) calculations of photoabsorption spectra for pyrazine (a) and the real and imaginary parts of the survival amplitudes in (b) and (c), respectively, according to benchmark simulations based on the 4-D model Hamiltonian. TT-SOFT simulations are labeled with the values of their corresponding accuracy parameters, either ε = 0.02 (gray line) or ε = 0.01 (dashed black line).

thereby, illustrating the dynamically adaptive nature of the TT-SOFT representation.

Figure 3 shows the experimental[45] photoabsorption spectrum of pyrazine as compared to the calculated spectrum based on TT-SOFT simulations of nonadiabatic dynamics for the 24-dimensional wavepacket evolving at the S_1/S_2 conical intersection. Spectra calculated with ε = 0.007 and ε = 0.006 exhibited close agreement with each other, differing at most by 0.029 in normalized intensity units.

The agreement is also reflected in the comparison of autocorrelation functions, shown in Figure 4. These results suggest that using an accuracy parameter of ε = 0.007 in TT-SOFT calculations yields sufficiently converged results for this system. Furthermore, both spectra exhibited agreement with the measured spectrum, as obtained with a modest number of tensor elements (e.g., 301 648 elements in the 24-dimensional

DOI: 10.1021/acs.jctc.7b00608
J. Chem. Theory Comput. XXXX, XXX, XXX−XXX

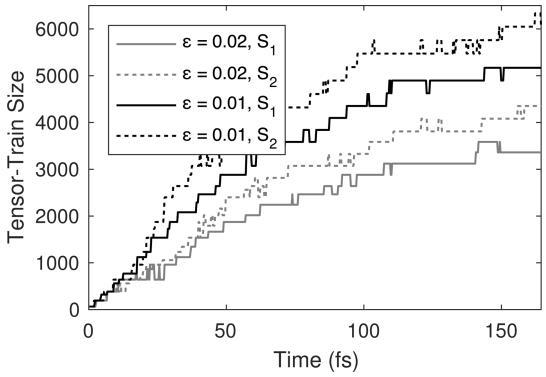

Figure 2. Number of elements in the tensor-train representations of the time-evolving wave functions corresponding to each electronic surface (S_1 and S_2) for the two 4-D TT-SOFT calculations with ε = 0.02 or ε = 0.01.

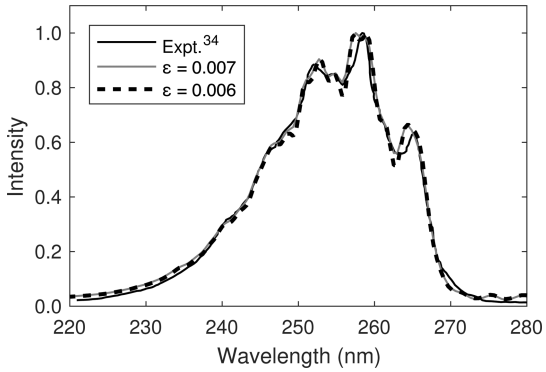

Figure 3. Normalized photoabsorption spectra for pyrazine, as calculated using TT-SOFT with the 24-D Hamiltonian with accuracy parameters of ε = 0.007 (solid gray line) and ε = 0.006 (dashed black line) and as measured experimentally in ref 45 (solid black line).

TT representation of the S_2 wavepacket after the final propagation step, compared to 7.92×10^{28} elements in what would be the corresponding full-rank representation with the same grid). The 24-dimensional TT-SOFT simulation finished in less than 4 h, thus demonstrating the efficiency with which multidimensional wave functions can be manipulated in the TT format.

4. CONCLUSIONS

We have introduced the TT-SOFT method for nonadiabatic quantum dynamics simulations of multidimensional wavepackets. We have demonstrated its accuracy and capabilities as applied to the simulation of the S_1/S_2 intersystem crossing in pyrazine. The TT-SOFT approach represents the 24-dimensional wavepacket of pyrazine on a grid and propagates it with the Trotter expansion of the time-evolution operator, just like in the standard SOFT method. However, it avoids the exponential scaling by keeping the time-evolving wavepacket in the tensor-train format. The size of the representation is dynamically adapted, as updated after each propagation step by a series of SVDs truncated with a single (user-specified) accuracy parameter.

We have evaluated the accuracy and efficiency of TT-SOFT through calculation of the photoabsorption spectrum of pyrazine. The calculations involved propagation of the 24-dimensional nuclear wave functions evolving on the two coupled electronic surfaces, as described by a vibronic

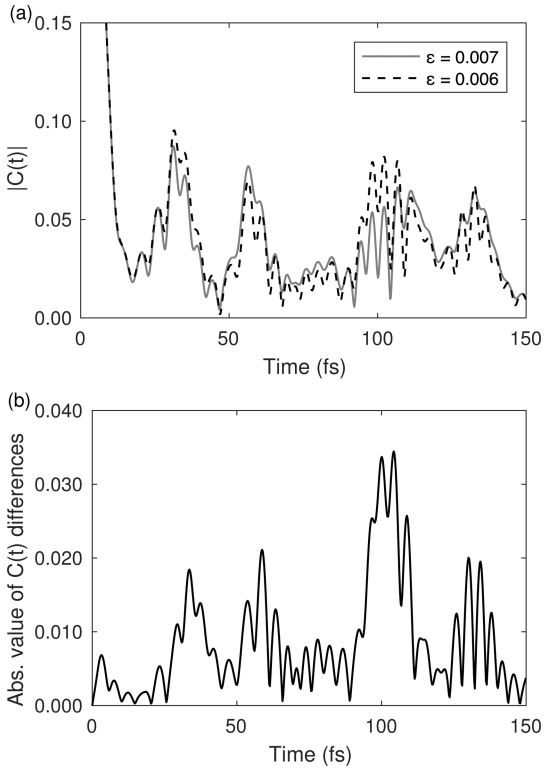

Figure 4. (a) Absolute value of the autocorrelation functions $|C(t)|$ from the ε = 0.007 and ε = 0.006 24-D TT-SOFT calculations. (b) Absolute value of the difference between these autocorrelation functions.

Hamiltonian. The reported simulations based on the propagation of the 24-dimensional wavepackets and benchmark calculations for a 4-dimensional model Hamiltonian demonstrated that the TT-SOFT method is a rigorous and powerful approach for simulations of multidimensional nonadiabatic quantum dynamics.

AUTHOR INFORMATION

Corresponding Author

*(V.S.B.) E-mail: victor.batista@yale.edu.

ORCID

Victor S. Batista: 0000-0002-3262-1237

Funding

V.S.B. acknowledges support from the NSF Grant CHE-1465108 and high-performance computing time from National Energy Research Scientific Computing Center (NERSC) and the Yale High Performance Computing Center. S.M.G. acknowledges supercomputer time from the Yale HPC Center.

Notes

The authors declare no competing financial interest.

REFERENCES

(1) Althorpe, S. C.; Clary, D. C. Quantum Scattering Calculations on Chemical Reactions. *Annu. Rev. Phys. Chem.* **2003**, *54*, 493−529.

(2) Parker, D.; Minns, R.; Penfold, T.; Worth, G.; Fielding, H. Ultrafast dynamics of the S_1 excited state of benzene. *Chem. Phys. Lett.* **2009**, *469*, 43−47.

(3) Hartland, G. V. Optical Studies of Dynamics in Noble Metal Nanostructures. *Chem. Rev.* **2011**, *111*, 3858−3887.

DOI: 10.1021/acs.jctc.7b00608
J. Chem. Theory Comput. XXXX, XXX, XXX−XXX

(4) Richter, M.; Marquetand, P.; González-Vázquez, J.; Sola, I.; González, L. Femtosecond Intersystem Crossing in the DNA Nucleobase Cytosine. *J. Phys. Chem. Lett.* **2012**, *3*, 3090−3095.
(5) Chergui, M. On the interplay between charge, spin and structural dynamics in transition metal complexes. *Dalton Trans.* **2012**, *41*, 13022−13029.
(6) Sjulstok, E.; Olsen, J. M. H.; Solov'yov, I. A. Quantifying electron transfer reactions in biological systems: what interactions play the major role? *Sci. Rep.* **2016**, *5*, 18446.
(7) High, J. S.; Rego, L. G. C.; Jakubikova, E. Quantum Dynamics Simulations of Excited State Energy Transfer in a Zinc-Free-Base Porphyrin Dyad. *J. Phys. Chem. A* **2016**, *120*, 8075−8084.
(8) Feit, M. D.; Fleck, J. A.; Steiger, A. Solution of the Schrödinger-equation by a spectral method. *J. Comput. Phys.* **1982**, *47*, 412.
(9) Feit, M. D.; Fleck, J. A. Solution of the Schrödinger equation by a spectral method *II*: *V*ibrational energy levels of triatomic molecules. *J. Chem. Phys.* **1983**, *78*, 301.
(10) Kosloff, D.; Kosloff, R. A Fourier method solution for the time dependent Schrödinger equation as a tool in molecular dynamics. *J. Comput. Phys.* **1983**, *52*, 35−53.
(11) Meyer, H.; Gatti, F.; Worth, G. *Multidimensional Quantum Dynamics: MCTDH Theory and Applications*; John Wiley & Sons: 2009.
(12) Nyman, G.; Yu, H.-G. Quantum approaches to polyatomic reaction dynamics. *Int. Rev. Phys. Chem.* **2013**, *32*, 39−95.
(13) Park, T. J.; Light, J. C. Unitary quantum time evolution by iterative Lanczos reduction. *J. Chem. Phys.* **1986**, *85*, 5870−5876.
(14) Tal-Ezer, H.; Kosloff, R. An accurate and efficient scheme for propagating the time dependent Schrödinger equation. *J. Chem. Phys.* **1984**, *81*, 3967.
(15) Chen, R.; Guo, H. The Chebyshev propagator for quantum systems. *Comput. Phys. Commun.* **1999**, *119*, 19−31.
(16) Burant, J. C.; Batista, V. S. Real time path integrals using the Herman−Kluk propagator. *J. Chem. Phys.* **2002**, *116*, 2748−2756.
(17) Guallar, V.; Batista, V. S.; Miller, W. H. Semiclassical molecular dynamics simulations of intramolecular proton transfer in photo-excited 2−(2′-hydroxyphenyl)−oxazole. *J. Chem. Phys.* **2000**, *113*, 9510−9522.
(18) Wang, H.; Sun, X.; Miller, W. H. Semiclassical approximations for the calculation of thermal rate constants for chemical reactions in complex molecular systems. *J. Chem. Phys.* **1998**, *108*, 9726−9736.
(19) Wang, H.; Thoss, M.; Miller, W. H. Forward−backward initial value representation for the calculation of thermal rate constants for reactions in complex molecular systems. *J. Chem. Phys.* **2000**, *112*, 47−55.
(20) Shalashilin, D. V.; Child, M. S. Real time quantum propagation on a Monte Carlo trajectory guided grids of coupled coherent states: 26D simulation of pyrazine absorption spectrum. *J. Chem. Phys.* **2004**, *121*, 3563−3568.
(21) Shalashilin, D. V.; Child, M. S. Basis set sampling in the method of coupled coherent states: Coherent state swarms, trains, and pancakes. *J. Chem. Phys.* **2008**, *128*, 054102.
(22) Wu, Y.; Batista, V. S. Matching-pursuit for simulations of quantum processes. *J. Chem. Phys.* **2003**, *118*, 6720−6724.
(23) Ben-Nun, M.; Martínez, T. J. In *Advances in Chemical Physics*; Prigogine, I., Rice, S. A., Eds.; John Wiley & Sons, Inc: New York, NY, U.S.A., 2002; Vol. *121*; pp 439−512.
(24) Yang, S.; Coe, J. D.; Kaduk, B.; Martínez, T. J. An "optimal" spawning algorithm for adaptive basis set expansion in nonadiabatic dynamics. *J. Chem. Phys.* **2009**, *130*, 134113.
(25) Burghardt, I.; Giri, K.; Worth, G. Multimode quantum dynamics using Gaussian wavepackets: The Gaussian-based multiconfiguration time-dependent Hartree (G-MCTDH) method applied to the absorption spectrum of pyrazine. *J. Chem. Phys.* **2008**, *129*, 174104.
(26) Meyer, H.-D.; Manthe, U.; Cederbaum, L. S. The multi-configurational time-dependent Hartree approach. *Chem. Phys. Lett.* **1990**, *165*, 73−78.
(27) Beck, M.; Jäckle, A.; Worth, G.; Meyer, H.-D. The multi-configuration time-dependent Hartree (MCTDH) method: a highly efficient algorithm for propagating wavepackets. *Phys. Rep.* **2000**, *324*, 1−105.
(28) Meyer, H.-D.; Worth, G. A. Quantum molecular dynamics: propagating wavepackets and density operators using the multi-configuration time-dependent Hartree method. *Theor. Chem. Acc.* **2003**, *109*, 251−267.
(29) Worth, G. A.; Meyer, H.-D.; Köppel, H.; Cederbaum, L. S.; Burghardt, I. Using the MCTDH wavepacket propagation method to describe multimode non-adiabatic dynamics. *Int. Rev. Phys. Chem.* **2008**, *27*, 569−606.
(30) Wang, H. Multilayer Multiconfiguration Time-Dependent Hartree Theory. *J. Phys. Chem. A* **2015**, *119*, 7951−7965.
(31) Wang, H.; Thoss, M. Multilayer formulation of the multi-configuration time-dependent Hartree theory. *J. Chem. Phys.* **2003**, *119*, 1289−1299.
(32) Raab, A.; Worth, G. A.; Meyer, H.-D.; Cederbaum, L. S. Molecular dynamics of pyrazine after excitation to the S_2 electronic state using a realistic 24-mode model Hamiltonian. *J. Chem. Phys.* **1999**, *110*, 936−946.
(33) Wu, Y.; Batista, V. Matching pursuit for simulations of quantum processes. *J. Chem. Phys.* **2003**, *118*, 6720.
(34) Wu, Y.; Batista, V. Erratum: Matching Pursuit for Simulations of Quantum Processes [J. Chem. Phys. 118, 6720, 2003]. *J. Chem. Phys.* **2003**, *119*, 7606.
(35) Wu, Y.; Batista, V. Quantum tunneling dynamics in multi-dimensional systems: A matching-pursuit description. *J. Chem. Phys.* **2004**, *121*, 1676.
(36) Mallat, S.; Zhang, Z. Matching pursuits with time-frequency dictionaries. *IEEE T. Signal Proces.* **1993**, *41*, 3397.
(37) Oseledets, I. V. Tensor-Train Decomposition. *SIAM J. Sci. Comput.* **2011**, *33*, 2295−2317.
(38) Press, W. H.; Flannery, B. P.; Teukolsky, S. A.; Vetterling, W. T. *Numerical Recipes*; Cambridge University Press: Cambridge, 1986.
(39) Seidner, L.; Stock, G.; Sobolewski, A. L.; Domcke, W. *Ab initio* characterization of the $S_1 \rightarrow S_2$ conical intersection in pyrazine and calculation of spectra. *J. Chem. Phys.* **1992**, *96*, 5298−5309.
(40) Woywod, C.; Domcke, W.; Sobolewski, A. L.; Werner, H. Characterization of the S_1ĐS$_2$ conical intersection in pyrazine using *ab initio* multiconfiguration self-consistent-field and multireference configuration-interaction methods. *J. Chem. Phys.* **1994**, *100*, 1400−1413.
(41) Stock, G.; Woywod, C.; Domcke, W.; Swinney, T.; Hudson, B. S. Resonance Raman spectroscopy of the S_1 and S_2 states of pyrazine: Experiment and first principles calculation of spectra. *J. Chem. Phys.* **1995**, *103*, 6851−6860.
(42) Thoss, M.; Miller, W. H.; Stock, G. Semiclassical description of nonadiabatic quantum dynamics: Application to the S_1ĐS$_2$ conical intersection in pyrazine. *J. Chem. Phys.* **2000**, *112*, 10282−10292.
(43) Coletti, C.; Billing, G. D. Quantum dressed classical mechanics: application to the photo-absorption of pyrazine. *Chem. Phys. Lett.* **2003**, *368*, 289−298.
(44) Chen, L.; Gelin, M. F.; Chernyak, V. Y.; Domcke, W.; Zhao, Y. Dissipative dynamics at conical intersections: simulations with the hierarchy equations of motion method. *Faraday Discuss.* **2016**, *194*, 61−80.
(45) Yamazaki, I.; Murao, T.; Yamanaka, T.; Yoshihara, K. Intramolecular electronic relaxation and photoisomerization processes in the isolated azabenzene molecules pyridine, pyrazine and pyrimidine. *Faraday Discuss. Chem. Soc.* **1983**, *75*, 395−405.
(46) Innes, K.; Ross, I.; Moomaw, W. R. Electronic states of azabenzenes and azanaphthalenes: A revised and extended critical review. *J. Mol. Spectrosc.* **1988**, *132*, 492−544.
(47) Horio, T.; Fuji, T.; Suzuki, Y.-I.; Suzuki, T. Probing Ultrafast Internal Conversion through Conical Intersection via Time-Energy Map of Photoelectron Angular Anisotropy. *J. Am. Chem. Soc.* **2009**, *131*, 10392−10393.
(48) Suzuki, Y.-I.; Fuji, T.; Horio, T.; Suzuki, T. Time-resolved photoelectron imaging of ultrafast $S_2 \rightarrow S_1$ internal conversion through conical intersection in pyrazine. *J. Chem. Phys.* **2010**, *132*, 174302.

DOI: 10.1021/acs.jctc.7b00608
J. Chem. Theory Comput. XXXX, XXX, XXX−XXX

(49) Suzuki, T. Ultrafast Internal Conversion of Aromatic Molecules Studied by Photoelectron Spectroscopy using Sub-20 fs Laser Pulses. *Molecules* **2014**, *19*, 2410−2433.
(50) Kolda, T. G.; Bader, B. W. Tensor Decompositions and Applications. *SIAM Rev.* **2009**, *51*, 455−500.
(51) Higham, N. J. The Scaling and Squaring Method for the Matrix Exponential Revisited. *SIAM Rev.* **2009**, *51*, 747−764.
(52) Chen, X.; Batista, V. S. Matching-pursuit/split-operator-Fourier-transform simulations of excited-state nonadiabatic quantum dynamics in pyrazine. *J. Chem. Phys.* **2006**, *125*, 124313.

DOI: 10.1021/acs.jctc.7b00608
J. Chem. Theory Comput. XXXX, XXX, XXX−XXX